Feature Article

Finite-Difference Time-Domain (FD-TD) Modeling of Electromagnetic Wave Scattering and Interaction Problems

by

Allen Taflove
EECS Department
Northwestern University
Evanston, IL 60201

Korada R. Umashankar
EECS Department
University of Illinois at Chicago
Chicago, IL 60680

Abstract- This article, based upon invited papers at the XXII URSI General Assembly (Tel Aviv, August 1987) and the URSI National Radio Science Meeting (Boulder, January 1988), reviews recent applications of the finite-difference time-domain (FD-TD) method for numerical modeling of electromagnetic wave scattering and interaction problems. One of the goals of this article is to demonstrate that recent advances in FD-TD modeling concepts and software implementation, combined with advances in computer technology, have expanded the scope, accuracy, and speed of FD-TD modeling to the point where it may be the preferred choice for structures that cannot be easily treated by conventional integral equation and asymptotic approaches. As a class, such structures are electrically large and have complex shapes, material compositions, apertures, and interior cavities.

1. INTRODUCTION

Contemporary high-frequency electromagnetic engineering problems can involve wave interactions with complex, electrically-large three-dimensional structures. These structures can have shapes, material compositions, apertures, or cavities which produce near fields that cannot be resolved into finite sets of modes or rays. Proper numerical modeling of such near fields requires sampling at subwavelength resolution to avoid aliasing of magnitude and phase information. The goal is to provide a self-consistent model of the mutual coupling of the electrically small cells comprising the structure.

A candidate numerical modeling approach for this purpose is the finite-difference time-domain (FD-TD) solution of Maxwell's curl equations. This approach is analogous to existing finite-difference solutions of fluid flow problems encountered in computational aerodynamics, in that the numerical model is based upon a direct solution of the governing partial differential equation. Pursuing this analogy, FD-TD shares the computational requirements of the fluids codes (and other similar large-scale partial differential equation solvers) in terms of computer floating point arithmetic rate, primary random access memory size, and data bandwidth to secondary memory. Yet, FD-TD is a non-traditional approach to numerical electromagnetic modeling, where frequency-domain approaches have dominated.

One of the goals of this article is to demonstrate that recent advances in FD-TD modeling concepts and software implementation, combined with advances in computer technology, have expanded the scope, accuracy and speed of FD-TD modeling to the point where it may be the preferred choice for certain types of scattering and coupling problems. With this in mind, this article will succinctly review the following recent FD-TD modeling validations and research frontiers:

Continued on page 6

Introducing Feature Article Author

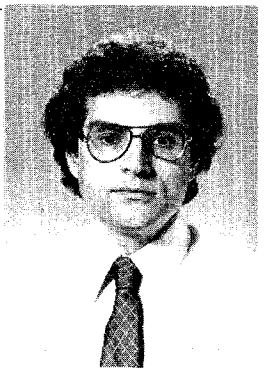

Allen Taflove

Allen Taflove was born in Chicago, IL on June 14, 1949. He received the B.S. (with highest distinction), M.S., and Ph.D. degrees in electrical engineering from Northwestern University, Evanston, IL, in 1971, 1972, and 1975, respectively.

From 1975 to 1984, he was a staff member at IIT Research Institute in Chicago, IL, holding the positions of Associate Engineer, Research Engineer, and Senior Engineer. There, in addition to research in electromagnetic wave scattering and penetration, he provided technical leadership for major programs in joint right-of-way design for 60-Hz transmission lines and pipelines or railroads; and extraction of oil from shale, tar sand, and slowly producing wells using novel in situ electromagnetic heating technology. He is one of three principal co-inventors of the latter, and has been granted 10 U.S. patents in this area.

In 1984, Dr. Taflove returned to Northwestern as an Associate Professor in the EECS Department. Since then, he has developed several research programs in analysis and numerical methods for electromagnetic wave interactions with large, complex structures. His related interests include inverse scattering / target synthesis; applications of recent vector supercomputers and concurrent processors in computational electromagnetics; and the new on-surface radiation condition (OSRC) theory for high-frequency scattering, which he originated along with G. A. Kriegsmann and K. R. Umashankar.

Dr. Taflove is a member of Tau Beta Pi, Eta Kappa Nu, and Sigma Xi. He is a Senior Member of IEEE and a member of URSI Commission B.

Feature Article—*Continued from page 5*

1. Scattering models for three-dimensional reentrant structures spanning up to 9 wavelengths;
2. Conformal models of curved surfaces;
3. Scattering models for two-dimensional anisotropic structures;
4. Penetration models for narrow slots and lapped joints in thick screens;
5. Coupling models for wires and wire bundles in free space and in arbitrary metal cavities;
6. Penetration models for the electromagnetic fields within detailed, inhomogeneous tissue approximations of the complete human body (at UHF frequencies);
7. Microstrip and microwave circuit models;
8. Scattering models for relativistically vibrating mirrors;
9. Inverse scattering reconstruction of one-dimensional, spatially coincident profiles of electrical permittivity and conductivity;
10. Inverse scattering reconstruction of two-dimensional conducting, homogeneous, and inhomogeneous dielectric targets from minimal TM scattered field pulse response data; and
11. Large-scale computer software.

Introducing Feature Article Author

Korada R. Umashankar

Korada R. Umashankar received the B.E. degree from Mysore University, India, in 1962; the M.E. degree from the Indian Institute of Science, Bangalore, India, in 1964; and the Ph.D. degree from the University of Mississippi, University, MS, in 1974; all in electrical engineering.

From 1964 to 1969, he was Assistant Professor and Head of the Department of Electrical Engineering, College of Engineering, Karnatak University, Hubli, India. During 1974 and 1975, he was a Postdoctoral Research Associate, and from 1975 to 1977, Assistant Professor of Electrical Engineering at the University of Mississippi. From 1977 to 1979, he was the National Research Council Visiting Fellow at the U. S. Air Force Weapons Laboratory, Kirtland AFB, NM. During 1979 to 1984, he was Senior Engineer at IIT Research Institute, Chicago, IL.

Currently, Dr. Umashankar is Associate Professor of Electrical Engineering and Computer Science at the University of Illinois at Chicago. His primary research is in the development of analytical and numerical techniques in electromagnetic theory, EMP / EMC interactions, and EM simulation studies. Research topics include the study of scattering from bodies comprised of, or coated with, anisotropic media; extension of the method of moments to electrically very large targets; and the new on-surface radiation condition (OSRC) theory for high-frequency scattering.

Dr. Umashankar is a member of Eta Kappa Nu and Sigma Xi. He is a Senior Member of IEEE and a member of URSI Commission B.

2. GENERAL CHARACTERISTICS OF FD-TD

As stated, FD-TD is a direct solution of Maxwell's time-dependent curl equations. It employs no potentials. Instead, it applies simple, second-order accurate central-difference approximations [1] for the space and time derivatives of the electric and magnetic fields directly to the respective differential operators of the curl equations. This achieves a sampled-data reduction of the continuous electromagnetic field in a volume of space, over a period of time. Space and time discretizations are selected to bound errors in the sampling process, and to insure numerical stability of the algorithm [2]. Electric and magnetic field components are interleaved in space to permit a natural satisfaction of tangential field continuity conditions at media interfaces. Overall, FD-TD is a marching-in-time procedure which simulates the continuous actual waves by sampled-data numerical analogs propagating in a data space stored in a computer. At each time step, the system of equations to update the field components is fully explicit, so that there is no need to set up or solve a set of linear equations, and the required computer storage and running time is proportional to the electrical size of the volume modeled.

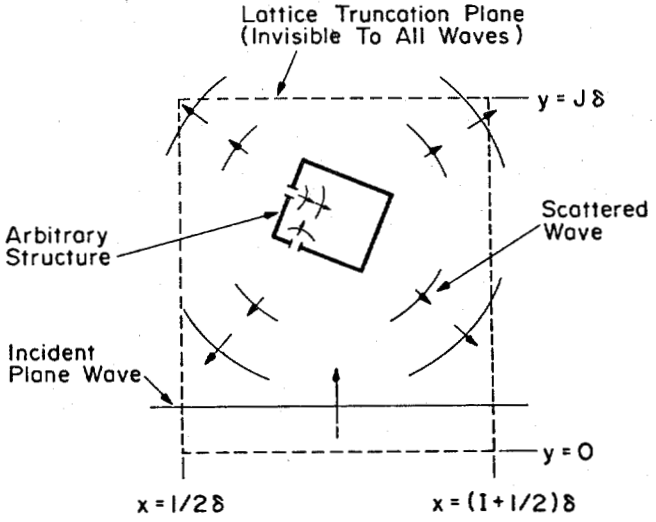

Figure 1. Time-Domain Wave-Tracking Concept of the FD-TD Method

Fig. 1 illustrates the time-domain wave tracking concept of the FD-TD method. A region of space within the dashed lines is selected for field sampling in space and time. At time = 0, it is assumed that all fields within the numerical sampling region are identically zero. An incident plane wave is assumed to enter the sampling region at this point. Propagation of the incident wave is modeled by the commencement of time stepping, which is simply the implementation of the finite-difference analog of the curl equations. Time stepping continues as the numerical analog of the incident wave strikes the modeled target embedded within the sampling region. All outgoing

Continued on page 7

Feature Article—*Continued from page 6*

scattered wave analogs ideally propagate through the lattice truncation planes with negligible reflection to exit the sampling region. Phenomena such as induction of surface currents, scattering and multiple scattering, penetration through apertures, and cavity excitation are modeled time-step by time-step by the action of the curl equations analog. Self-consistency of these modeled phenomena is generally assured if their spatial and temporal variations are well resolved by the space and time sampling process.

Time stepping is continued until the desired late-time pulse response or steady-state behavior is achieved. An important example of the latter is the sinusoidal steady state, wherein the incident wave is assumed to have a sinusoidal dependence, and time stepping is continued until all fields in the sampling region exhibit sinusoidal repetition. This is a consequence of the limiting amplitude principle [3]. Extensive numerical experimentation with FD-TD has shown that the number of complete cycles of the incident wave required to be time-stepped to achieve the sinusoidal steady state is approximately equal to the Q factor of the structure or phenomenon being modeled.

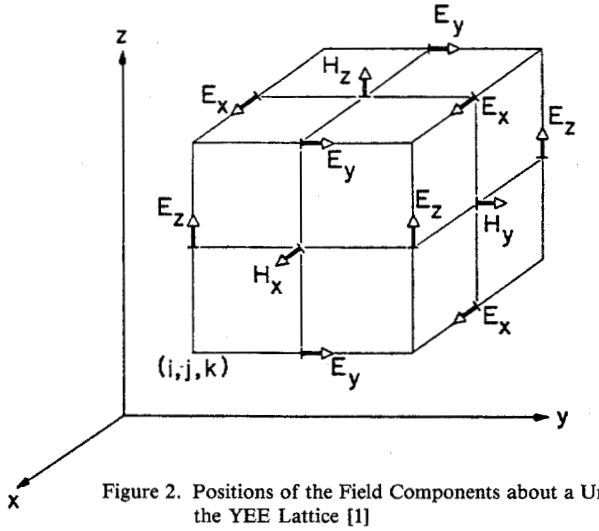

Figure 2. Positions of the Field Components about a Unit Cell of the YEE Lattice [1]

Fig. 2 illustrates the positions of the electric and magnetic field components about a unit cell of the FD-TD lattice in Cartesian coordinates [1]. Note that each magnetic field vector component is surrounded by four circulating electric field vector components, and vice versa. This arrangement permits not only a centered-difference analog to the space derivatives of the curl equations, but also a natural geometry for implementing the integral form of Faraday's Law and Ampere's Law at the space-cell level. This integral interpretation permits a simple but effective modeling of the physics of smoothly curved target surfaces, penetration through narrow slots having sub-cell gaps, and coupling to thin wires having sub-cell diameters, as will be seen later.

Fig. 3 illustrates how an arbitrary three-dimensional scatterer is embedded in an FD-TD space lattice comprised of the unit cells of Fig. 2. Simply, desired values of electrical permittivity and conductivity are assigned to each electric field component of the lattice. Correspondingly, desired values of magnetic permeability and equivalent conductivity are assigned to each magnetic field component of the lattice. The media parameters are interpreted by the FD-TD program as local coefficients for the time-stepping algorithm. Specification of media properties in this component-by-component manner

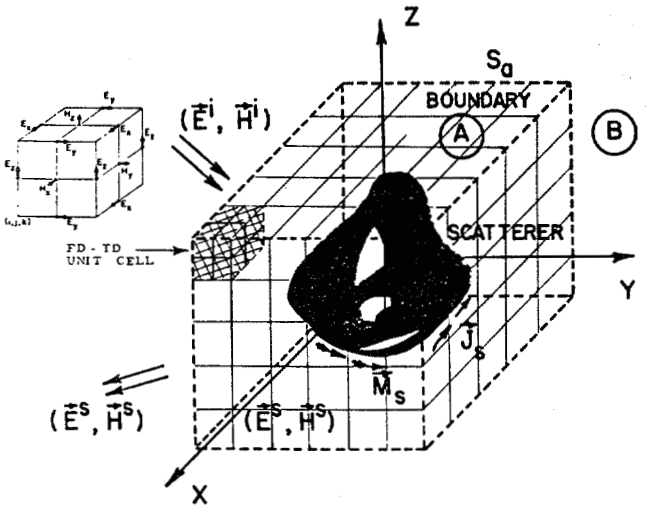

Figure 3. Arbitrary Three-Dimensional Scatterer Embedded in a FD-TD Lattice

results in a stepped-edge, or staircase, approximation of curved surfaces. Continuity of tangential fields is assured at the interface of dissimilar media with this procedure. There is no need for special field matching at media interface points. Stepped-edge approximation of curved surfaces has been found to be adequate in the FD-TD modeling problems studied in the 1970's and early 1980's, including wave interactions with biological tissues [4], penetration into cavities [5], [6], and electromagnetic pulse (EMP) interactions with complex structures [7]-[9]. However, recent interest in wide dynamic range models of scattering by curved targets has prompted the development of surface-conforming FD-TD approaches which eliminate staircasing. These will be summarized later in this article.

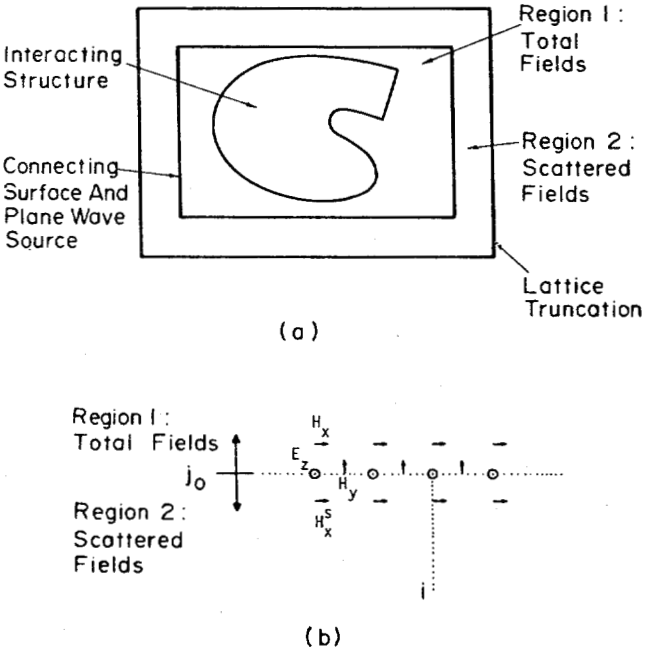

Figure 4. Division of FD-TD Lattice into Total-Field and Scattered-Field Regions. (a) Lattice division; (b) Field component geometry at connecting plane y = $j_o\delta$ [10], [11]

Fig. 4 illustrates the division of the FD-TD lattice into total-field and scattered-field regions. This division has been found to be very useful since it permits the efficient simulation of an incident plane wave in the total-field region with arbitrary

Continued on page 8

Feature Article—*Continued from page 7*

angle of incidence, polarization, time-domain waveform, and duration [10], [11]. Three additional important benefits arise from this lattice division.

a. A large near-field computational dynamic range is achieved, since the scatterer of interest is embedded in the total-field region. Thus, low field levels in shadow regions or within shielding enclosures are computed directly without suffering subtraction noise (as would be the case if scattered fields in such regions were time-stepped via FD-TD, and then added to a cancelling incident field to obtain the low total-field levels).

b. Embedding the scatterer in the total-field region permits a natural satisfaction of tangential field continuity across media interfaces, as discussed earlier, without having to compute the incident field at possibly numerous points along a complex locus that is unique to each scatterer. The zoning arrangement of Fig. 4 requires computation of the incident field only along the rectangular connecting surface between the total-field and scattered-field regions. This surface is fixed, i.e., independent of the shape or composition of the enclosed scatterer being modeled.

c. The provision of a well-defined scattered-field region in the FD-TD lattice permits the near-to-far field transformation illustrated in Fig. 5. The dashed virtual surface shown in Fig. 5 can be located along convenient lattice planes in the scattered-field region of Fig. 4. Tangential scattered E and H fields computed via FD-TD at this virtual surface can then be weighted by the free-space Green's function and then integrated (summed) to provide the far-field response and radar cross section (full bistatic response for the assumed illumination angle) [11] - [13]. The near-field integration surface has a fixed rectangular shape, and thus is independent of the shape or composition of the enclosed scattered being modeled.

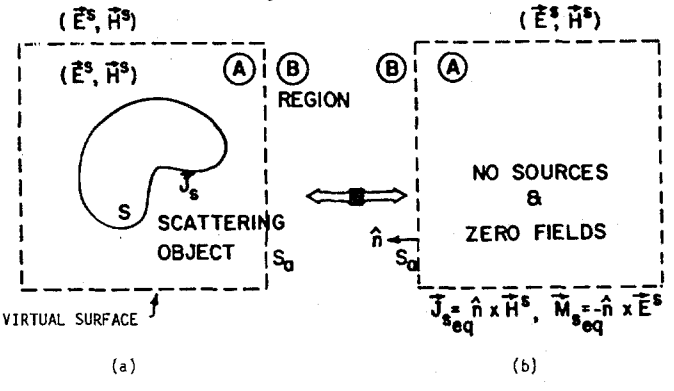

Figure 5. Near-to-Far Field Transformation Geometry
(a) Original problem; (b) Equivalent problem external to the virtual surface, S_a [11]

Fig. 4 uses the term "lattice truncation" to designate the outermost lattice planes in the scattered-field region. The fields at these planes cannot be computed using the centered-differencing approach discussed earlier because of the assumed absence of known field data at points outside of the lattice truncation. These data are needed to form the central differences. Therefore, an auxiliary lattice truncation condition is necessary. This condition must be consistent with Maxwell's equations in that an outgoing scattered-wave numerical analog striking the lattice truncation must exit the lattice without appreciable non-physical reflection, just as if the lattice truncation was invisible. It has been shown that the required lattice truncation condition is really a radiation condition in the near field [10], [14] - [17]. Further, it has been shown that convenient local approximations of the exact radiation condition can be generated and applied with good results [10] - [17]. Based upon this research, the procedure for constructing more precise local approximations of the exact radiation condition is reasonably well understood. These approximations are currently under study for numerical implementation in the FD-TD computer programs [18].

3. THREE-DIMENSIONAL FD-TD SCATTERING MODELS

Analytical and experimental validations have been obtained relative to FD-TD modeling of canonical three-dimensional conducting targets spanning 1/3 to 9 wavelengths [12], [13], [19], [20]. For brevity, only one such validation will be reviewed here.

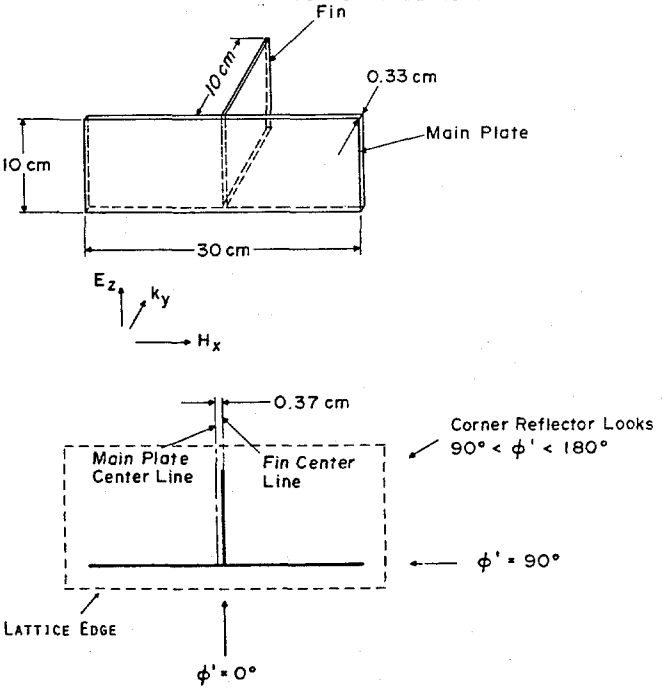

Fig. 6. Geometry of Crossed-Plate Scatterer and Illumination [13], [19], [20]

Fig. 6 depicts the geometry of a crossed-plate scatterer comprised of two flat plates electrically bonded together to form the shape of a "T". The main plate has the dimensions 30 cm x 10 cm x 0.33 cm, and the bisecting fin has the dimensions 10 cm x 10 cm x 0.33 cm. The illumination is a plane wave at 0° elevation angle and TE polarization relative to the main plate, and at the frequency 9.0 GHz. Thus, the main plate spans 9.0 wavelengths. Note that look angle azimuths between 90° and 180° provide substantial corner reflector physics, in addition to the edge diffraction, corner diffraction, and other effects found for an isolated flat plate.

For the 9-GHz FD-TD model, the lattice cell size is 0.3125 cm, approximately 1/11 wavelength. The main plate is formed by 32 x 96 x 1 cells; the bisecting fin is formed by 32 x 32 x 1 cells; and the overall lattice is comprised of 48 x 112 x 48 cells (1,548,288 unknown field components) containing 212.6 cubic

Continued on page 9

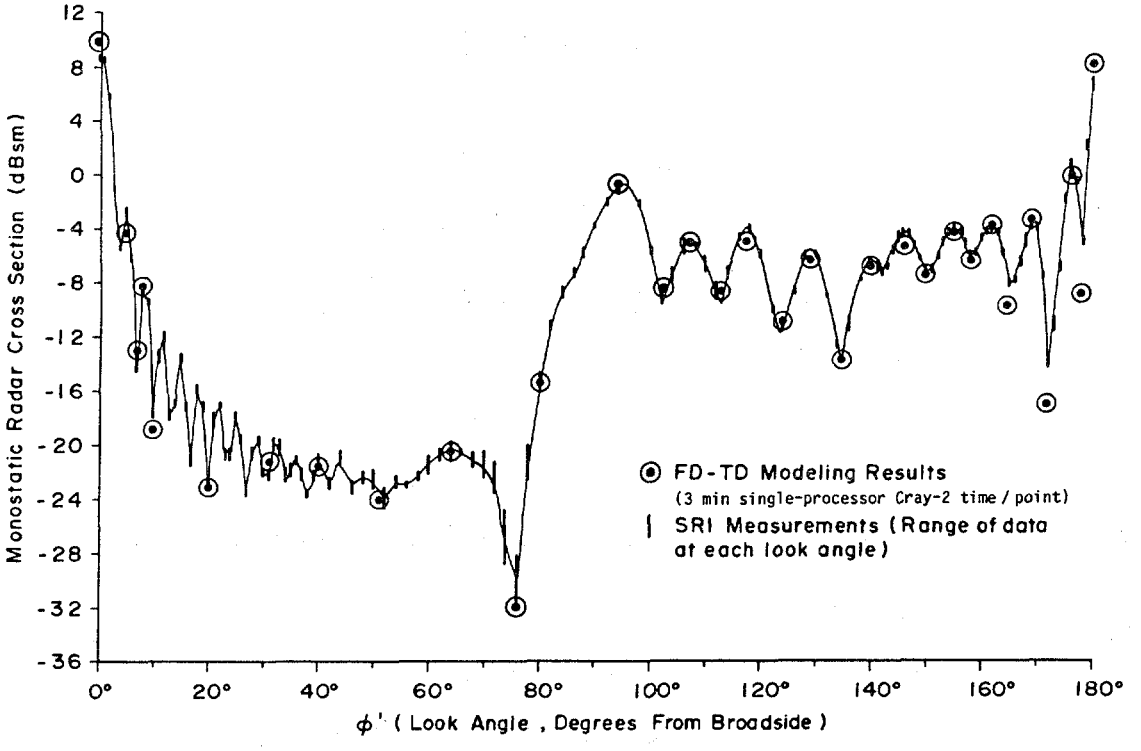

Fig. 7. Comparison of FD-TD Modeling with SRI Measurements of Monostatic Radar Cross Section for the Crossed-Plate Scatterer at 9 GHZ (maximum scatterer size = 9 wavelengths) [13], [19], [20]

wavelengths. Note that the lattice truncations are only 8 cells (0.75 wavelength) from the target's main plate and fin edges. The slightly eccentric positioning of the bisecting fin is accounted for in the FD-TD model. Starting with zero-field initial conditions, 661 time steps are used, equivalent to 31 cycles of the incident wave at 9 GHz.

Measurements of the monostatic radar cross section (RCS) vs. look angle azimuth were performed in the anechoic chamber facility operated by SRI International, Menlo Park, CA. Fig. 7 compares the FD-TD predictions with the SRI measurements at 32 key look angles which define the major features of the RCS response. It is seen that the agreement is within about 1 dB over a total RCS-pattern dynamic range of 40 dB. Locations of peaks and nulls of the pattern are accurately predicted to within 1° of azimuth. Note especially the excellent agreement for look angle azimuths greater than 90°, where there is a pronounced corner-reflector effect. As stated in [13], it appears that this case (and similar three-dimensional 9-wavelength targets studied in [20]) represents the largest detailed three-dimensional numerical scattering models of any type ever verified wherein a uniformly fine spatial resolution and the ability to treat nonmetallic composition is incorporated in the model.

4. TWO-DIMENSIONAL CONFORMAL MODELS OF CURVED SURFACES

A key flaw in previous FD-TD models of conducting structures with smooth curved surfaces has been the need to use stepped-edge (staircase) approximations of the actual structure surface. Although not a serious problem for computing wave penetration and coupling into low-Q metal cavities, recent FD-TD studies have shown that stepped approximations of curved walls and aperture surfaces can shift center frequencies of resonant responses by 1% to 2% for Q factors of 30 to 80, and can possibly introduce spurious nulls. In the area of scattering and RCS, the use of stepped surfaces has prevented application of FD-TD for modeling the important class of targets where surface roughness, exact curvature, and dielectric or permeable loading is crucial in determining RCS.

Recently, two different types of FD-TD conformal surface models have been proposed and examined for two-dimensional problems:

a. Faraday's Law contour path models [21]. These preserve the basic Cartesian grid arrangement of field components at all space cells except those adjacent to the target surface. Space cells adjacent to the surface are deformed to conform with the surface locus. Slightly modified time-stepping expressions for the magnetic field components adjacent to the surface are derived from the integral form of Faraday's Law implemented around the perimeters of the deformed cells.

b. Stretched, conforming mesh models [22], [23]. These employ available numerical mesh generation schemes to construct non-Cartesian grids which are continuously stretched to conform with smoothly shaped targets. Time-stepping expressions are either adapted from the Cartesian FD-TD case [22] or obtained via analogy to the computational fluid dynamics (CFD) case [23].

Research is ongoing for each of these types of conformal surface models. Key questions include: ease of mesh generation; suppression of numerical artifacts such as instability, dispersion, and nonphysical wave reflections; coding complexity; and modeling execution time.

Continued on page 10

Feature Article—*Continued from page 9*

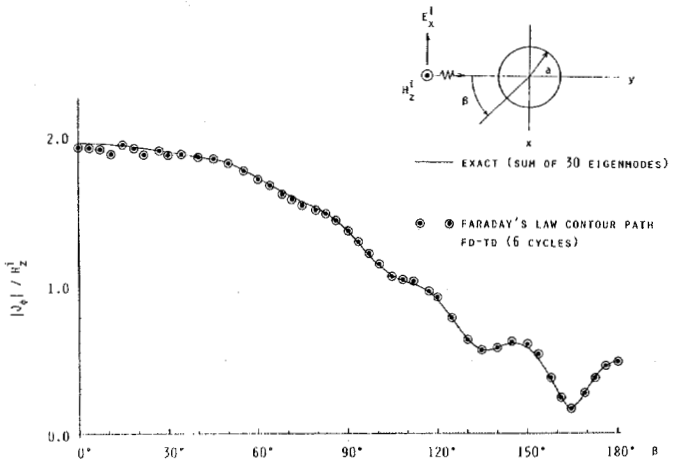

Fig. 8. Comparison of FD-TD and Exact Solution for Azimuthal Surface Electric Current on a ka = 5 Circular Conducting Cylinder, TM Case (0.05 wavelength grid cell size) [21]

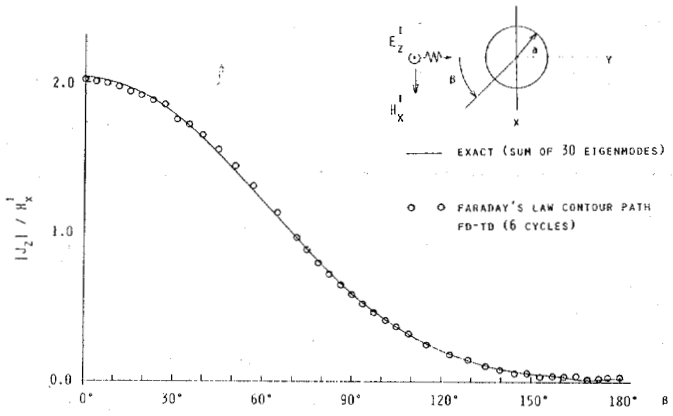

Fig. 9. Comparison of FD-TD and Exact Solution for Longitudinal Surface Electric Current on a Ka = 5 Circular Conducting Cylinder, TM Case (0.05 wavelength grid cell size) [21]

The accuracy of the Faraday's Law contour path models for smoothly curved targets subjected to TE and TM illumination is illustrated in Figs. 8 and 9, respectively. Here, a moderate-resolution Cartesian FD-TD grid (having 1/20 wavelength cell size) is used to compute the azimuthal or longitudinal current distribution on the surface of a ka = 5 circular metal cylinder. For both polarizations, the contour path FD-TD model achieves an accuracy of 1.5% or better at most surface points relative to the exact series solution. The worst-case error, only 3.5%, occurs for the TE case at a point in the center-lit region where contour deformation is maximum. Running time for the conformal FD-TD model is essentially the same as for the old staircase FD-TD model, since only a few H components immediately adjacent to the target surface require a slightly modified time-stepping relation.

5. SCATTERING MODELS FOR TWO-DIMENSIONAL ANISOTROPIC STRUCTURES

The ability to independently specify electrical permittivity and conductivity for each E vector component in the FD-TD lattice, and magnetic permeability and equivalent conductivity for each H vector component, leads immediately to the possibility of using FD-TD to model material targets having diagonal-tensor electric and magnetic properties. No alteration of the basic FD-TD algorithm is required. The more complicated behavior associated with off-diagonal tensor components can also be modeled, in principal, with some algorithm complications [20].

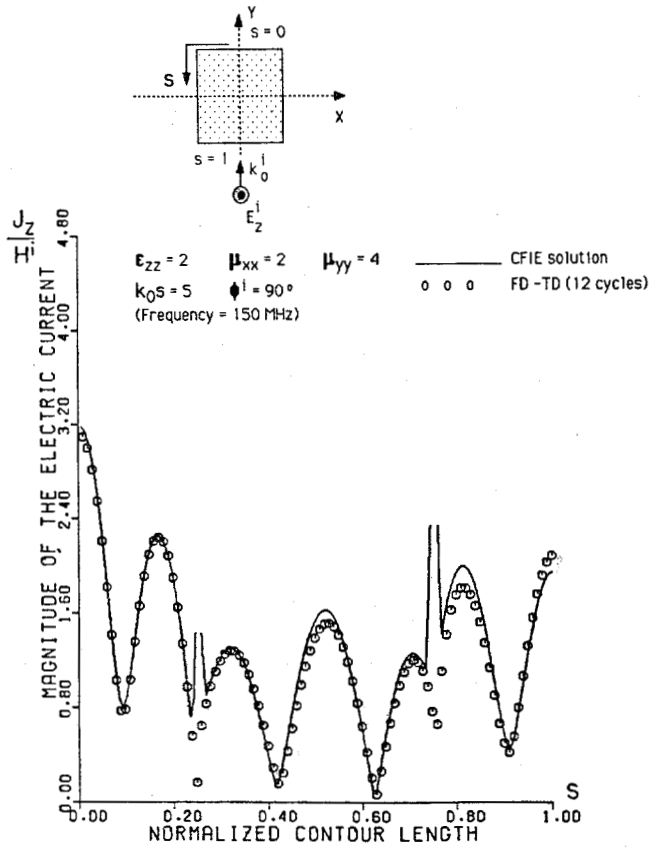

Fig. 10. Comparison of FD-TD and CFIE Solutions for Longitudinal Surface Electric Current on A $K_0 s = 5$ Square Anisotropic Cylinder, TM Case [24]

Recent development of combined-field, coupled surface integral equations for modeling scattering by arbitrary shaped two-dimensional anisotropic targets [24] has permitted detailed tests of the accuracy of FD-TD anisotropic models. Fig. 10 illustrates one such test. Here, the magnitude of the equivalent surface electric current induced by TM illumination of a square anisotropic cylinder is graphed as a function of position along the cylinder surface for both the FD-TD and combined-field integral equation (CFIE) models. The incident wave propagates in the +y direction and has a +z-directed electric field. The cylinder has an electrical size $k_0 s = 5$, permittivity $\epsilon_{zz} = 2$, and diagonal permeability tensor $\mu_{xx} = 2$ and $\mu_{yy} = 4$. From Fig. 10, we see that the FD-TD and CFIE results agree very well over almost everywhere on the cylinder surface. Disagreement is noted at the cylinder corners where CFIE predicts sharp local peaks whereas FD-TD predicts local nulls. Studies are continuing to resolve the corner physics issue.

6. PENETRATION MODELS FOR NARROW SLOTS AND LAPPED JOINTS IN THICK SCREENS

The physics of electromagnetic wave transmission through narrow slots and lapped joints in shielded enclosures must be accurately understood to permit

Continued on page 11

Feature Article—*Continued from page 10*

good engineering design of equipment to meet specifications for performance concerning electromagnetic pulse (EMP), lightning, high-power microwaves (HPM), electromagnetic interference and compatibility (EMI and EMC), undesired radiated signals, and RCS. In many cases, slots and joints may have very narrow gaps filled by air, oxidation films, or layers of anodization or paint. Joints can be simple (say, two metal sheets butted together); more complex (a lapped or "furniture" joint); or even more complex (a threaded screw-type connection with random points of metal-to-metal contact, depending upon the tightening). Extra complications arise from the possibility of electromagnetic resonances within the joint, either in the transverse or longitudinal (depth) direction.

Clearly, to make any headway with this complicated group of problems using the FD-TD approach, it is necessary to develop and validate FD-TD models which can simulate the geometric features of generic slots and joints. Since a key geometric feature is likely to be the narrow gap of the slot or joint relative to one FD-TD space cell, it is important to understand how sub-cell gaps can be efficiently modeled.

Three different types of FD-TD sub-cell models have been proposed and examined for modeling narrow slots and joints:

a. Equivalent slot loading [25]. Here, rules are set to define an equivalent permittivity and permeability in a slot formed by a single-cell gap to effectively narrow the gap to the desired degree.

b. Subgridding [26]. Here, the region within the slot or joint is provided with a sufficiently fine grid. This grid is properly connected to the coarser grid outside of the slot.

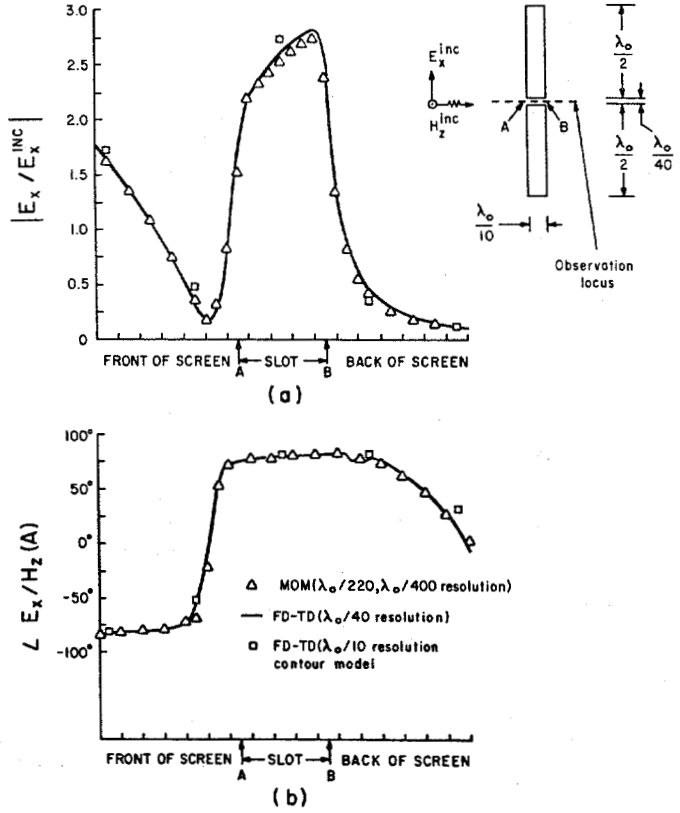

Fig. 11. Comparison of FD-TD and MOM Solutions for the Gap Electric Field Distribution, Straight Slot Case: (a) Magnitude; (b) Phase [27]

c. Faraday's Law contour path model [27]. Here, space cells adjacent to and within the slot or joint are deformed to conform with the surface locus (in a manner similar to the conformal curved surface model). Slightly modified time-stepping expressions for the magnetic field components in these cells are derived from the integral form of Faraday's Law implemented around the perimeters of the deformed cells.

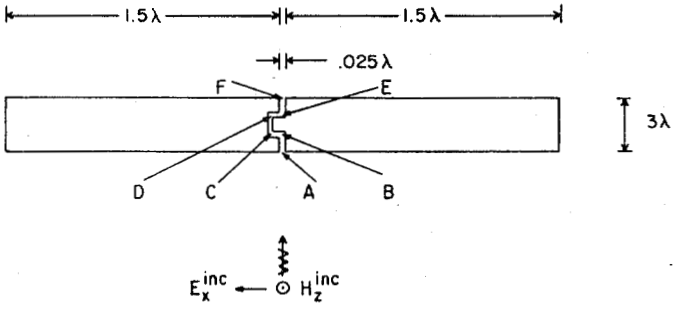

Fig. 12(a)

Fig. 12a. Geometry of U-Shaped Lapped Joint For TE Illumination, Shown to Scale [27]

The accuracy of the Faraday's Law contour path model for narrow slots and joints is illustrated in Figs. 11 and 12 by direct comparison of the computed gap electric field against high-resolution numerical benchmarks. Fig. 11 models a 0.1 wavelength thick conducting screen which extends 0.5 wavelength to each side of a straight slot which has a gap of 0.025 wavelength. Broadside TE illumination is assumed. Three types of predictive data are compared: (1) The low-resolution (0.1 wavelength) FD-TD model using the contour path approach to treat the slot as a 1/4-cell gap; (2) A high-resolution (0.025 wavelength) FD-TD model to treat the slot as a 1-cell gap; and (3) A high-resolution method of moments (MOM) model (having 0.0025 wavelength sampling in the slot) which treats the slotted screen as a pure scattering geometry. From Fig. 11, we see that there is excellent agreement between all three sets of predictive data in both magnitude and phase. Of particular interest is the ability of the low-resolution FD-TD model, using the contour path approach, to accurately compute the peak electric field in the slot.

Continued on page 12

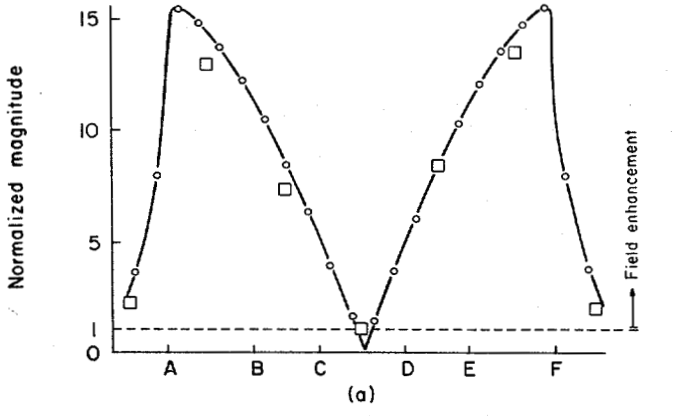

Feature Article—*Continued from page 11*

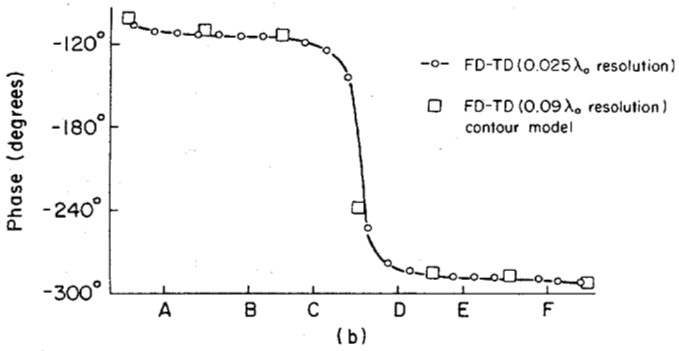

Fig. 12b. FD-TD Computed Gap Electric Field Within the 0.45-Wavelength Path Length, U-Shaped Lapped Joint (First Transmission Resonance): (a) $|E_{gap}/E_{inc}|$; (b) $\angle E_{gap}/H_z(A)$ [27]

Fig. 12a shows the geometry of a U-shaped lapped joint which was selected for detailed study of path-length (depth) power transmission resonances. The U shape of the joint permits adjustment of the overall joint path length without disturbing the positions of the input and output ports at A and F. A uniform gap of 0.025 wavelength is assumed, as is a screen thickness of 0.3 wavelength and width of 3 wavelengths. Fig. 12b compares the gap electric field within the joint as computed by: (1) A low-resolution, contour path FD-TD model having 0.09 wavelength cell size and treating the gap as 0.28 cell; and (2) A high-resolution FD-TD model having 0.025 wavelength cell size and treating the gap as 1 cell. The total path length within the lapped joint is adjusted to equal 0.45 wavelength, which provides a sharp power transmission peak to the shadow side of the screen. From Fig. 12b, we see a very good agreement between the low and high resolution FD-TD models, even though this is a numerically stressful, resonant penetration case. An implication of these results is that coarse (0.1 wavelength) FD-TD gridding can be effectively used to model the fine-grained physics of wave penetration through slots and joints, if simple algorithm modifications are made in accordance with the contour path approach. This can substantially reduce computer resource requirements and coding complexity for FD-TD models of complex structures, without sacrificing appreciable accuracy in the modeling results.

7. COUPLING MODELS FOR WIRES AND WIRE BUNDLES

In equipment design for EMP, HPM, and EMI / EMC, understanding electromagnetic wave coupling to wires and cable bundles located within shielding enclosures is a problem that is complementary to that of wave penetration through apertures of the shield (such as narrow slots and joints). Similar to the narrow slot problem, a key dimension of the interacting structure, in this case the wire or bundle diameter, may be small relative to one FD-TD space cell. Thus, it is important to understand how thin, sub-cell, wires and bundles can be efficiently modeled if FD-TD is to have much application to coupling problems.

Two different types of FD-TD sub-cell models have been proposed and examined for modeling thin wires:

a. Equivalent inductance [28]. Here, an equivalent inductance is defined for a wire within a space cell, permitting a lumped-circuit model of the wire to be set up and computed.

b. Faraday's Law contour path model [29]. Here, space cells adjacent to the wire are deformed to conform with the surface locus (in a manner similar to the conformal curved surface model). 1/r singularities of the azimuthal magnetic field and radial electric field are assumed to exist within the deformed cells. Slightly modified time-stepping expressions for the azimuthal magnetic field components in these cells are derived from the integral form of Faraday's Law implemented around the perimeter of the deformed cells.

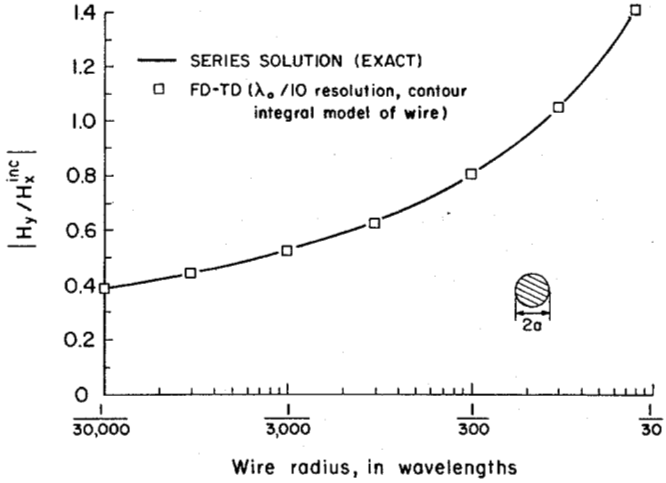

Fig. 13. Comparison of FD-TD and Exact Solution for the Scattered Azimuthal Magnetic Field at a Point 1/20 Wavelength From the Center of an Infinite Wire [29]

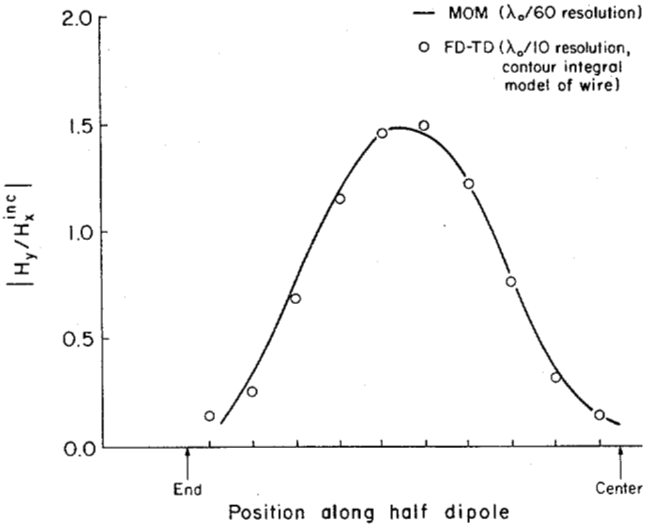

Fig. 14. Comparison of FD-TD and MOM Solutions for the Scattered Azimuthal Magnetic Field Distribution Along a 2.0-Wavelength Wire of Radius 1/300 Wavelength (Broadside TM illumination) [29]

The accuracy of the Faraday's Law contour path model for thin wires in free space is illustrated in Figs. 13 and 14. Fig. 13 graphs the scattered azimuthal magnetic field at a fixed distance of 1/20 wavelength from the center of an infinitely long wire having a radius ranging between 1/30,000 and 1/30 wavelength. TM illumination is assumed. We see that there is excellent agreement between the exact series solution and the low-resolution (0.1 wavelength) FD-TD contour path model over the entire 3-decade range of wire radius. Fig. 14 graphs the scattered azimuthal magnetic field distribution along a 2.0-wavelength (antiresonant) wire of radius 1/300 wavelength. Broadside TM illumination is assumed, and the field is observed at a fixed distance of 1/20 wavelength from

Continued on page 13

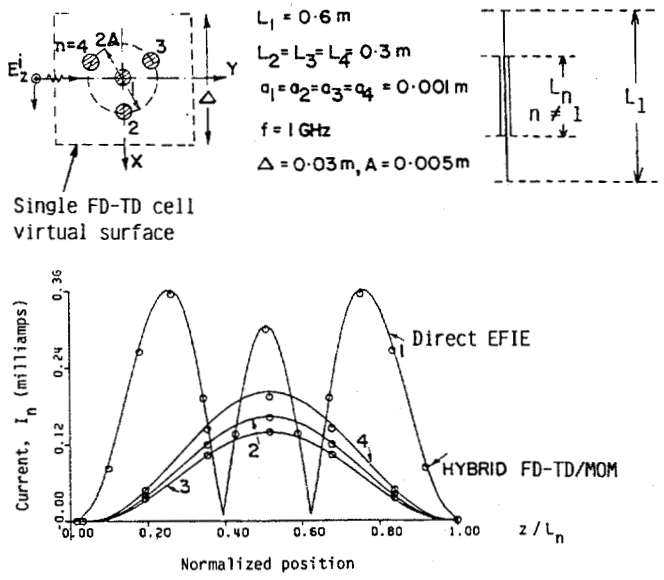

Fig. 15. Comparison of Hybrid FD-TD / MOM Modeling Predictions with Direct EFIE for Induced on a Wire Bundle Illuminated Broadside by a Plane Wave in Free Space [29]

Feature Article—*Continued from page 12*

the wire center. We see that there is excellent agreement between a MOM solution sampling the wire current at 1/60 wavelength increments, and the low-resolution (0.1 wavelength) FD-TD contour path model.

The FD-TD contour path model can be extended to treat thin wire bundles, as well as single wires. Fig. 15 shows the analytical validation results for the induced currents on a bundle comprised of 4 wires, where 3 are of equal length. Here, a wire of length 0.6 m (2.0 wavelengths) is assumed at the center of the bundle, and three parallel wires of length 0.3 m (1.0 wavelength) are assumed to be located at 120° separations on a concentric circle of radius 0.005 m (1/60 wavelength). The radii of all wires in the bundle are equal and set to 0.001 m (1/300 wavelength). The assumed excitation is in free space, provided by a 1-GHz broadside TM plane wave. Following the technique of [29], the bundle is replaced by a single wire having varying equivalent radius corresponding to the three sections along the bundle axis. The physics of the single wire of varying equivalent radius is incorporated in a low-resolution (0.1 wavelength) FD-TD contour path model, as discussed above. The FD-TD model is then run to obtain the tangential E and H fields at a virtual surface conveniently located at the cell boundary containing the equivalent wire (shown as a dashed line in Fig. 15). These fields are then utilized as excitation to obtain the currents induced on the individual wires of the original bundle. This last step is performed by setting up an electric field integral equation (EFIE) and solving via MOM. Fig. 15 shows an excellent correspondence between the results of the hybrid FD-TD / MOM procedure described above and the usual direct EFIE solution for the induced current distribution on each wire of the bundle.

The hybrid FD-TD / MOM procedure for modeling thin wire bundles is most useful when the bundle is located within a shielding enclosure. Fig. 17 shows the experimental validation results for the variation of induced load current with frequency for a single wire and a wire-pair located at the center of the cylindrical enclosure depicted in Fig. 16 [29]. The enclosure is 1.0 m high, 0.2 m in diameter, and referenced to a large metal ground plane. Approximate plane wave excitation is provided by an electrically-large conical monopole referenced to the same ground plane.

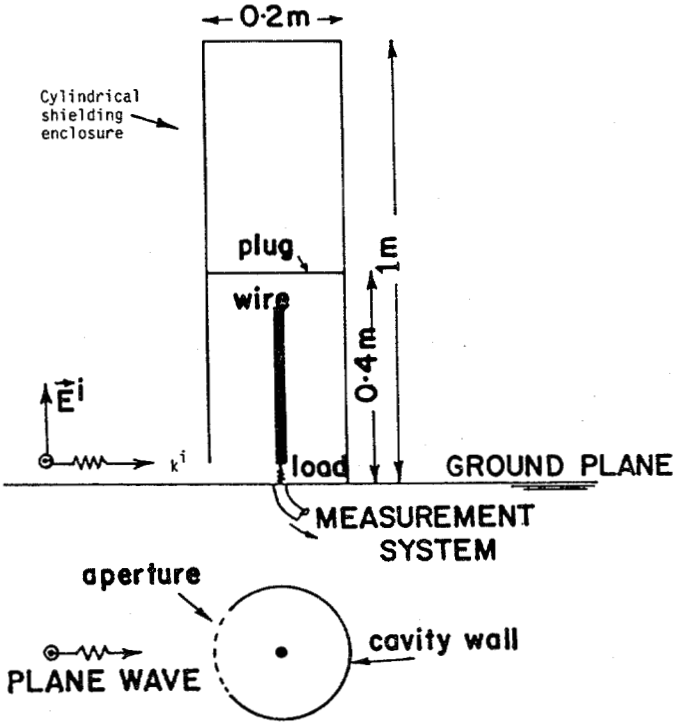

Fig. 16. Geometry of the Cylindrical Shielding Enclosure and Internal Wire or Wire-Pair [29]

Wave penetration into the interior of the enclosure is through a circumferential slot aperture (0.125 m arc length, 0.0125 m gap) at the ground plane. For the cases studied, an internal shorting plug is located 0.40 m above the ground plane. For the single-wire test, a wire of length 0.30 m and radius 0.000495 m is centered within the interior and connected to the ground plane with a lumped 50-ohm load. For the wire-pair test, parallel wires of these dimensions are located 0.01 m apart, with one wire shorted to the ground plane and the other connected to the ground plane with a lumped 50-ohm load. All results are normalized to a 1 v/m incident wave electric field.

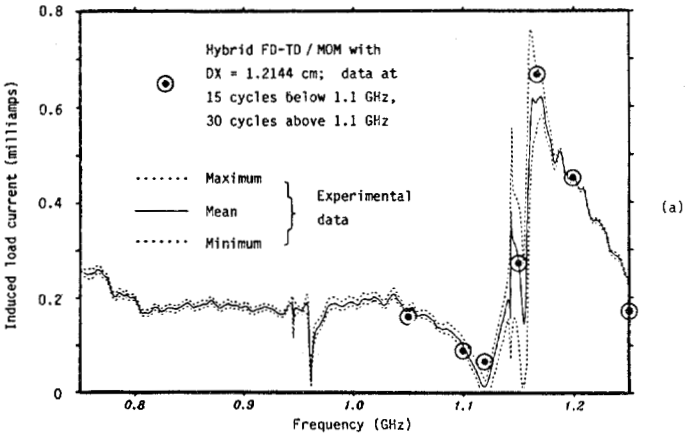

Fig. 17(a)

From Fig. 17, we see that there is a good correspondence between the measured and numerically modeled wire load current for both test cases. The two-wire test proved to be especially challenging since the observed Q factor of the coupling response (center

Continued on page 14

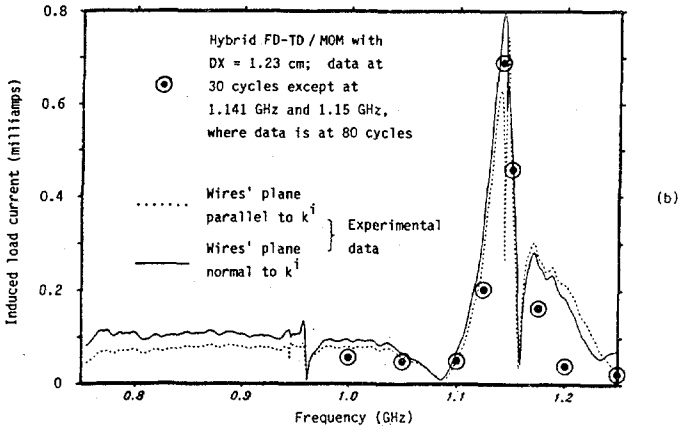

Fig. 17. Comparison of Hybrid FD-TD / MOM Modeling Predictions With Experimental Data For Induced Load Current: (a) Single Wire in Shielding Enclosure; (b) Wire-Pair in Shielding Enclosure [29]

Feature Article—*Continued from page 13*

frequency divided by the half-power bandwidth) is quite high, about 75. Indeed, it is found that the FD-TD code has to be stepped through as many as 80 cycles to approximately reach the sinusoidal steady state for excitation frequencies near the resonant peak. However, substantially fewer cycles of time stepping are needed away from the resonance, as indicated in the figure.

8. PENETRATION MODELS FOR BIOLOGICAL TISSUES

Two characteristics of FD-TD cause it to be very promising for modeling electromagnetic wave interactions with biological tissues: (1) Electrical media can be specified independently for each vector field component, so tissues of enormous complexity can be specified in principle; and (2) The required computer resources for this type of detailed volumetric modeling are dimensionally low, only of order N, where N is the number of space cells in the FD-TD lattice.

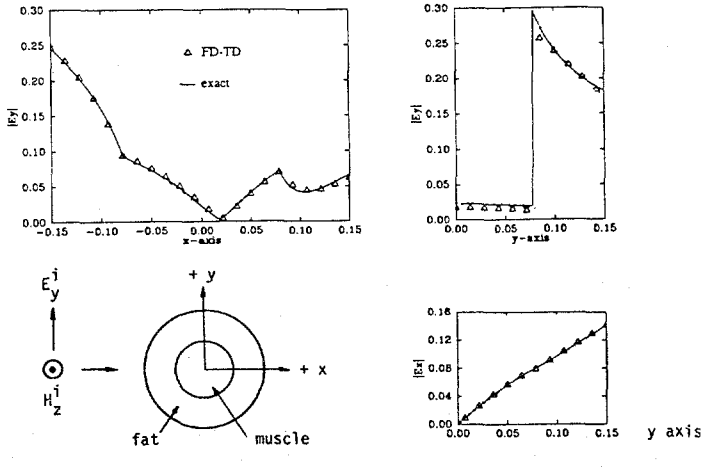

Fig. 18. Comparison of FD-TD and Exact Solution for Penetrating Electric Field Vector Components Within a Circular Muscle - Fat Layered Cylinder, TE Polarization, 100 MHZ [30]

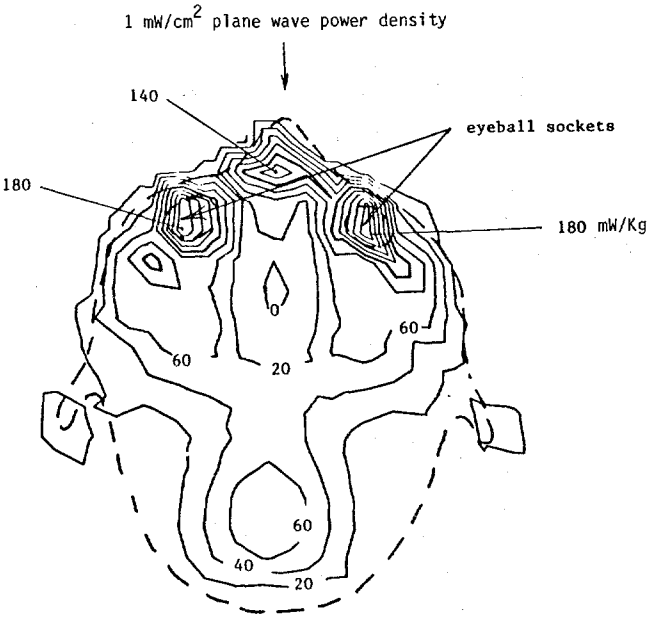

Fig. 19a. FD-TD Computed Contour Map of the Specific Absorption Rate (SAR) Distribution Along a Horizontal Cut Through the Head of the 3-D Inhomogeneous Man Model (350 MHZ) [32]

In fact, one of the earliest applications of FD-TD involved the construction of detailed inhomogeneous tissue models of the human eye to obtain predictive data for UHF / microwave penetration and heating [4].

The emergence of supercomputers has recently permitted FD-TD to be seriously applied to a number of important bio-electromagnetic problems. First, it was shown that FD-TD provides excellent agreement with series solutions for the penetrating field distributions within homogeneous and layered tissue cylinders and spheres [30], [31]. Fig. 18, taken from [30], shows the analytical validation results for the penetrating electric field vector components within a 0.15 m radius muscle-fat layered cylinder. The inner layer (radius = 0.079 m) is assumed to be comprised of muscle having a relative permittivity of 72 and conductivity of 0.9 S/m. The outer layer is assumed to be comprised of fat having a relative permittivity of 7.5 and conductivity of 0.048 S/m. TE illumination at a frequency of 100 MHz is modeled. From Fig. 18, we see that the FD-TD solution for the internal fields agrees very well with the exact solution, despite the fact that a stepped-edge (staircase) approximation of the circular layer boundaries is used.

After validation of FD-TD models of penetrating fields for canonical biological tissue shapes, attention turned toward modeling highly realistic inhomogeneous tissue approximations of the human body. Specific electrical parameters were assigned to each of the electric field vector components at the 16,000 to 40,000 space cells comprising the body model. Assignments were based upon cross-section tissue maps of the body (at spacings of about one inch, as obtained via cadaver studies) available in the medical literature, and cataloged measurements of tissue dielectric properties. Space resolutions as fine as 0.013 m throughout the entire human body proved possible using FD-TD. Figs. 19a and 19b, taken from [32], show the computed contour maps of the specific absorption rate (SAR) distribution along horizontal cuts through the head and liver, respectively, of the three-dimensional inhomogeneous man model. In Fig. 19a, the incident plane wave has a power density of 1 mW/cm^2 at 350 MHz, and each contour is 20 mW/Kg.

Continued on page 1.

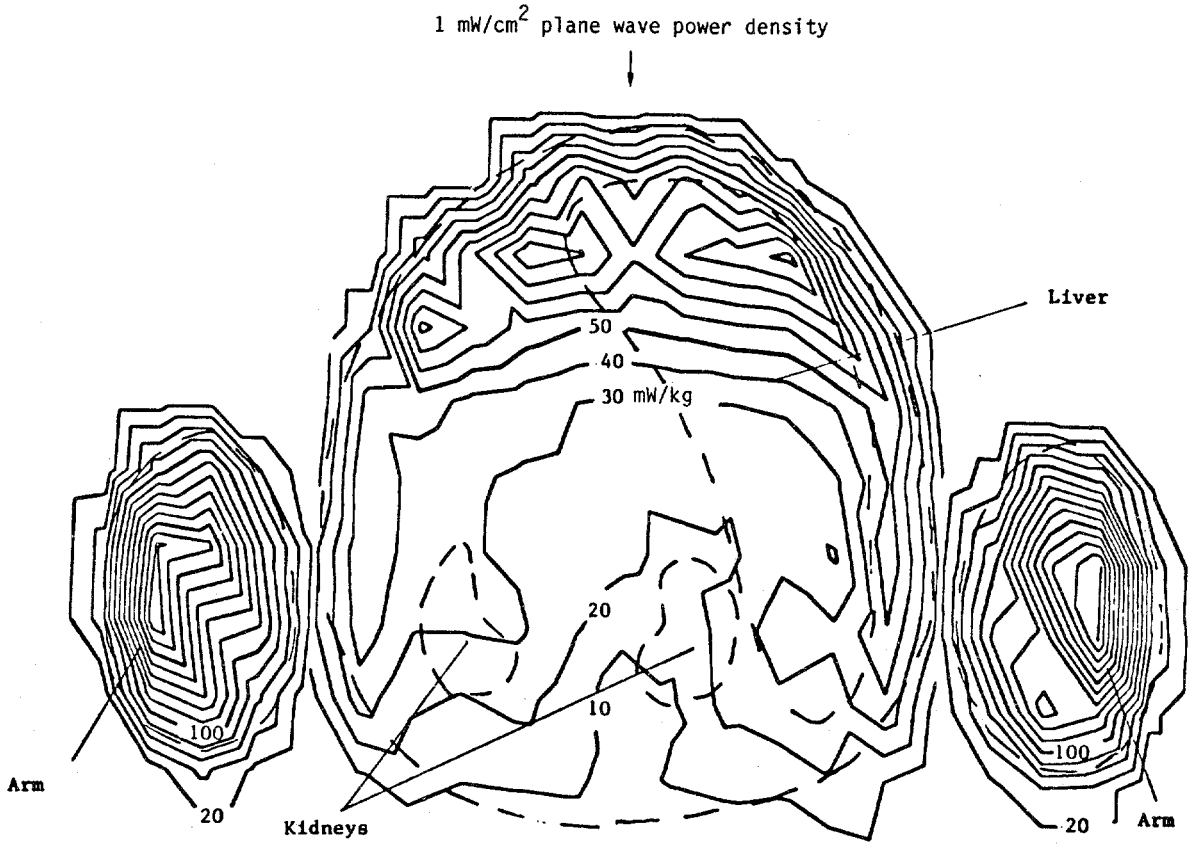

Fig. 19b. FD-TD Computed Contour Map of the Specific Absorption Rate (SAR) Distribution Along a Horizontal Cut Through the Liver of the 3-D Inhomogeneous Man Model (100 MHZ) [32]

Feature Article—*Continued from page 14*

In Fig. 19b, the incident wave has the same power density but is at 100 MHz; contours in the arms are at 20 mW/kg intervals, while contours in the body are at 10 mW/kg intervals. These contour maps illustrate the high level of detail of local features of the SAR distribution that is possible via FD-TD modeling.

More recent work has departed from simulations of plane wave illumination of the human body. Currently, FD-TD is being used to model annular phased arrays of aperture and dipole antennas used for hyperthermia [33]. A 17,363 cell, 0.013 m resolution, anatomically based model of the human torso surrounded by a bolus of deionized water is used for calculations of SARs. Test runs on the calculation of fields in the water-filled interaction space and with homogeneous circular and elliptical cylinder phantoms correlate well with the experimental data in the literature, lending support to the accuracy of the FD-TD method for near-field exposure conditions [33].

9. MICROSTRIP AND MICROWAVE CIRCUIT MODELS

Recently, FD-TD modeling has been extended to provide detailed characterizations of microstrips, resonators, finlines, and two-dimensional microwave circuits. In [34], FD-TD is used to calculate the dispersive characteristics of a typical microstrip on a gallium arsenide substrate. A Gaussian pulse excitation is used, and the effective dielectric constant and characteristic impedance vs. frequency is efficiently obtained over a broad frequency range via Fourier transform of the time-domain field response.

In [35], FD-TD is first used to obtain resonant frequencies of several three-dimensional cavities loaded by dielectric blocks. Next, the resonant frequency of a finline cavity is computed. Last, the resonant frequencies of a microstrip cavity on anisotropic substrate are obtained, and the dispersion characteristics of the microstrip used in the cavity are calculated. FD-TD modeling results are compared primarily to those obtained using the transmission line matrix (TLM) approach, and the two methods are found to give practically the same results.

Continued on page 16

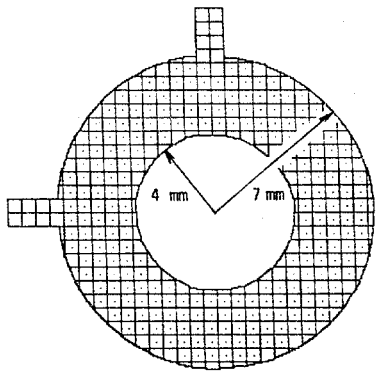

Fig. 20(a)

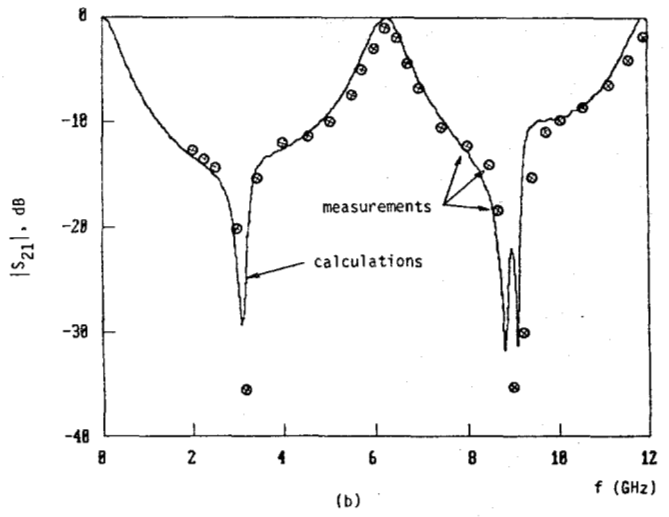

Fig. 20. Comparison of FD-TD Modeling Predictions With Measurements of $|S_{21}|$ for a Two-Port Microstrip Ring Circuit: (a) Geometry and Gridding of Microstrip Circuit; (b) Comparative Results Over 2 - 12 GHZ [36]

Feature Article—*Continued from page 15*

In [36], a modified version of FD-TD is presented which provides central-difference time-stepping expressions for distributions of voltage and surface current density along arbitrary-shaped two-dimensional microwave circuits. This approach is quite different from that of [34] and [35], which utilize the original volumetric field sampling concept for FD-TD. As a result, the method of [36] requires fewer unknowns to be solved, and avoids the need for a radiation boundary condition. However, an auxiliary condition is required to describe the loading effects of the fringing fields at the edges of the microstrip conducting paths. Fig. 20, taken from [36], shows the FD-TD computed S parameter, $|S_{21}|$, as a function of frequency for a two-port microstrip ring circuit. The ring circuit, gridded as shown in the figure, has an inner radius of 4 mm, outer radius of 7 mm, substrate relative permittivity of 10 and relative permeability of 0.93 (simulating duroid), and is connected to two 50-ohm lines making a 90° angle. The broadband response of the circuit is obtained using a single FD-TD run for an appropriate pulse excitation, followed by Fourier transformation of the desired response time-domain waveform. From Fig. 20, we see good agreement of the predicted and measured circuit response over the frequency range 2 - 12 GHz and a dynamic range of about 30 dB. [36] concludes that the application of its FD-TD approach to arbitrarily-shaped microstrip circuits is encouraging, but more work is needed to determine the modeling limitations, especially at higher frequencies where media dispersion can become important.

10. SCATTERING MODELS FOR RELATIVISTICALLY MOVING SURFACES IN ONE AND TWO DIMENSIONS

Analytical validations have been recently obtained for FD-TD models of reflection of a monochromatic plane wave by a perfectly conducting surface either moving at a uniform relativistic velocity or vibrating at a frequency and amplitude large enough so that the surface attains relativistic speeds [37]. The FD-TD approach of [37] is novel in that it does not require a system transformation where the conducting surface is at rest. Instead, the FD-TD grid is at rest in the laboratory frame, and the computed field solution is given directly in the laboratory frame. This is accomplished by implementing the proper relativistic boundary conditions for the fields at the surface of the moving conductor.

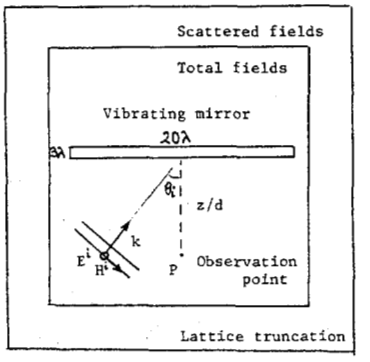

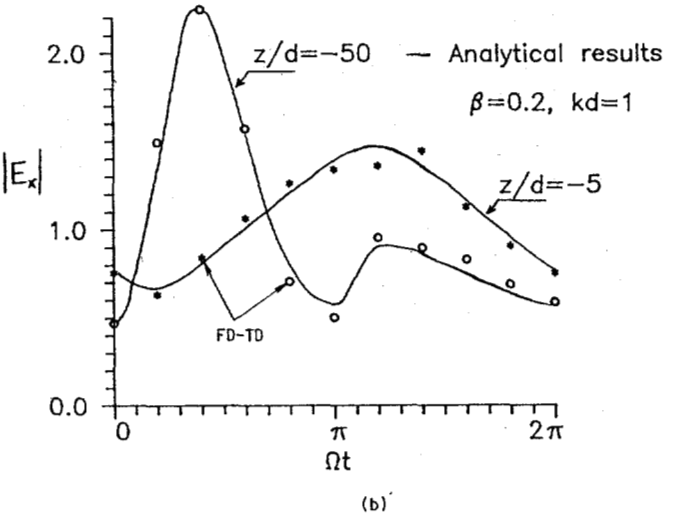

Fig. 21. Comparison of FD-TD and Analytical Results For the Envelope of the Scattered E Field VS. Time For a Monochromatic Plane Wave Illuminating a Vibrating Mirror at 30° [37]

Fig. 21 shows results for one of the more interesting problems of this type modeled so far, that of oblique plane wave incidence on an infinite vibrating mirror. This case is much more complicated than the normal incidence case, in that it has no closed-form solution. An analysis presented in the literature [38] writes the solution in an infinite series form using plane-wave expansions, where the unknown coefficients in the series are solved numerically. This analysis serves as the basis of comparison for the FD-TD model results for the time variation of the scattered field envelope at points near the mirror.

Since it is difficult to model exactly an infinite plane mirror in a finite two-dimensional grid, a long, thin, rectangular perfectly-conducting slab is used as the mirror model, as shown in Fig. 21a. Relativistic boundary conditions for the fields are implemented on the front and back sides of the slab. The other two sides, parallel to the velocity vector, are insensitive to the motion of the slab, and therefore no relativistic boundary conditions are required there. To minimize the impact of edge diffraction, the slab length is carefully selected so

Continued on page 17

Feature Article—*Continued from page 16*

that the slab appears to be infinite in extent at observation point, P, during a well-defined early-time response when the edge effect has not yet propagated to P. Since the TM case does not provide substantially different results than the TE case [38], only the TE case is considered. From Fig. 21b, we see good agreement between the FD-TD and analytical results obtained from [38] for the envelope of the scattered E field vs. time, for an incident angle of 30°, peak mirror speed 20% that of light, and observation points z/d = -5 and z/d = -50, where kd = 1. Similar agreement is found for an even more oblique angle, 60° [37]. This agreement is satisfying since the action of the relativistically vibrating mirror is so complicated, generating a reflected wave having a spread both in frequency and spatial reflection angle, as well as evanescent modes.

11. INVERSE SCATTERING RECONSTRUCTIONS IN ONE AND TWO DIMENSIONS

Initial work has demonstrated the possibility of accurately reconstructing one-dimensional profiles of permittivity and conductivity [39], and the shape and dielectric composition of two-dimensional targets [40], [41] from minimal scattered field pulse response data. The general approach involves setting up a numerical feedback loop which uses a one- or two-dimensional FD-TD code as a forward-scattering element, and a specially constructed nonlinear optimization code as the feedback element. FD-TD generates a test pulse response for a trial layering or target shape / composition. The test pulse is compared to the measured pulse, and an error signal is developed. Working on this error signal, the nonlinear optimization element perturbs the trial layering or target shape / composition in a manner to drive down the error. Upon repeated iterations, the proposed layering or target ideally converges to the actual one, a strategy similar to that of [42].

The advantage of working in the time domain is that a layered medium or target shape can be reconstructed sequentially in time as the wavefront of the incident pulse sweeps through, taking advantage of causality. This reduces the complexity of reconstruction since only a portion of the layering or target shape is being generated at each iteration. Advanced strategies for reconstruction in the presence of additive noise may involve the use of prediction / correction, where the trial layer or target shape is considered to be a predictor of the actual case, which is subsequently corrected by optimization of the entire layered medium or target using the complete scattered pulse.

Fig. 22 shows the application of the basic FD-TD feedback strategy to a one-dimensional layered medium in the absence of noise. Both the electrical permittivity and conductivity of the medium vary in a "sawtooth" manner with depth. The curves show simulated measured data for the reflected pulse for three cases defined by the peak values of the conductivity (0.001 S/m, 0.01 S/m, and 0.1 S/m) and the corresponding spatially coincident peak values of relative permittivity (3, 2, and 4) of the medium. In each case, the incident pulse is assumed to be a half-sinusoid spanning 50 cm between zero crossings. Noting that the dark dots superimposed on the "sawtooth" represent the reconstructed values of permittivity and conductivity, we see that the basic FD-TD feedback strategy is quite successful in the absence of noise [39].

Continued on page 18

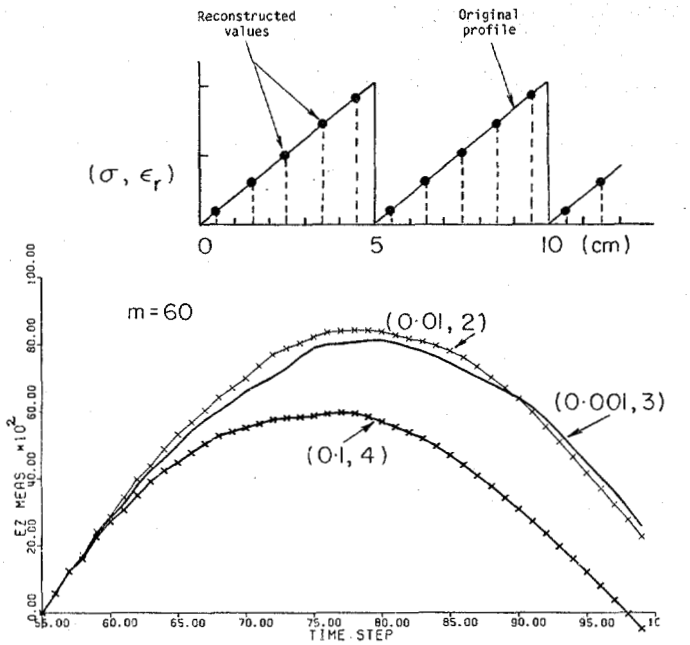

Fig. 22. Application of the FD-TD / Feedback Strategy to Reconstruct A 1-D Sawtooth Variation of Electrical Permittivity and Conductivity in the Absence of Noise [39]

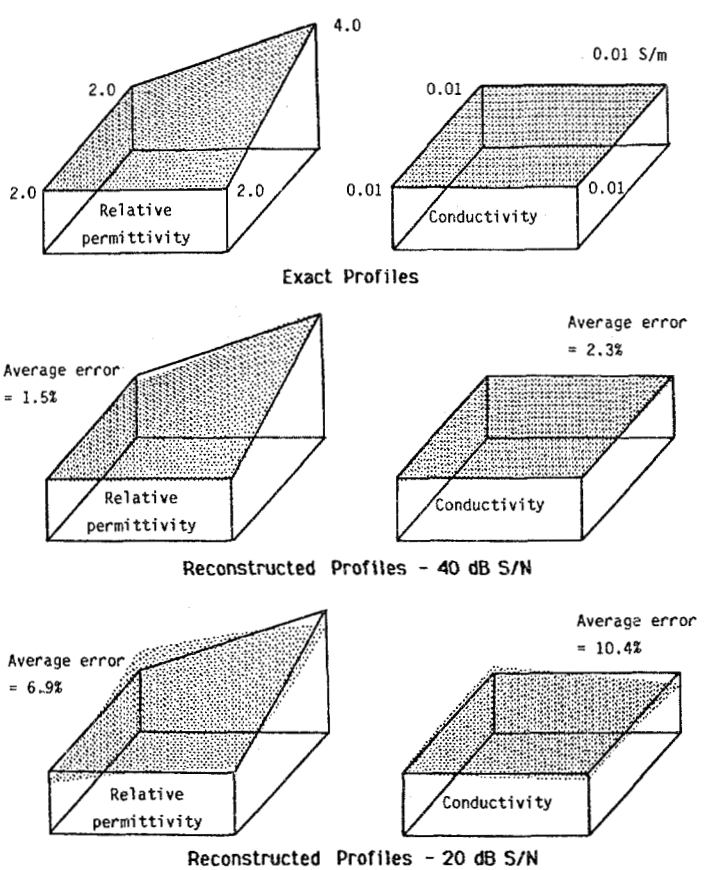

Fig. 23. Applications of the FD-TD / Feedback Strategy to Reconstruct a 2-D Lossy Dielectric Target in the Presence of Noise [41]

Feature Article—*Continued from page 17*

Fig. 23 shows the application of the FD-TD feedback strategy to reconstruct a two-dimensional lossy dielectric target. The target is a 30 cm x 30 cm square cylinder having a uniform conductivity of 0.01 S/m, and a tent-like relative permittivity profile which starts at 2.0 at the front and left sides and increases linearly to a peak value of 4.0 at the back corner on the right side. These profiles are illustrated in a perspective manner at the top of Fig. 23. The target is assumed to be illuminated by a TM polarized plane wave that is directed toward the front of the target (as visualized at the top of Fig. 23). The incident waveform is a 3-cycle sinusoidal tone burst having a 60-MHz carrier frequency. For the reconstruction, the only data utilized is the time-domain waveform of the scattered electric field as observed at two points. These points are located 1 m from the front of the target, and are positioned 15 cm to either side of the target center line. To simulate measured data, the computed scattered field waveforms are contaminated with additive Gaussian noise. In all of the reconstructions, the target shape and location is assumed to be known.

From Fig. 23, we see that for a signal/noise ratio of 40 dB, the average error in the permittivity and conductivity profiles is 1.5% and 2.3%, respectively. If the signal/noise ratio is reduced to 20 dB, the average errors increase to 6.9% and 10.4%, respectively [41]. Research is ongoing to determine means of improving the noise performance, especially using predictor/corrector techniques briefly discussed earlier. Given the relatively small amount of scattered field data utilized, the FD-TD feedback strategy appears promising for future development.

12. LARGE-SCALE COMPUTER SOFTWARE

The FD-TD method is naturally suited for large-scale processing by state-of-the-art vector supercomputers and concurrent processors. This is because essentially all of the arithmetic operations involved in a typical FD-TD run can be vectorized or cast into a highly concurrent format. Further, the O(N) demand for computer memory and clock cycles (where N is the number of lattice space cells) is dimensionally low, and permits three-dimensional FD-TD models spanning 50 - 100 wavelengths to be anticipated by 1990.

Let us now consider computation times of present FD-TD codes. Table 1 lists computation times (derived either from benchmark runs or based on analysts' estimates) for modeling one look angle of a 10-wavelength three-dimensional scatterer using the present FD-TD code. Four computing systems are listed in the table. The first is the Digital Equipment VAX 11/780, without floating point accelerator. The second and third are, respectively, single-processor and four-processor versions of the Cray-2. The fourth is a hypothetical next-generation machine operating at an average rate of 10 Gflops (10-billion floating point operations per second). This last computer is generally expected to be available about 1990 - 1992.

From Table 1, it is fairly clear that steadily advancing supercomputer technology will permit routine engineering usage of FD-TD for modeling electrically-large problems by the early 1990's.

An interesting prospect that has recently arisen is the reduction of the O(N) computational burden of FD-TD to $O(N^{1/3})$. This possibility is a consequence of the appearance of the Connection Machine (CM), which has tens of thousands of simple processors and

Table 1. Computation Times

Machine	10-Wavelength Model Present FD-TD Code*
VAX 11/780 (no floating point accelerator)	40.0 h
Cray-2 (single processor, using the VAX Fortran)	12.0 min
Cray-2 (single processor, some code optimization)	3.0 min
Cray-2 (four processors, some code optimization)	1 min (est.)
True 10 Gflop machine	2 sec (est.)

*$1.55 \cdot 10^6$ unknown field components, 661 time steps

associated memories arranged in a highly efficient manner for processor-to-procesor communication. With the CM, a single processor can be assigned to store and time-step a single row of vector field components in a three-dimensional FD-TD space lattice. For example, $1.5 \cdot 10^6$ processors would be sufficient to store the 6 Cartesian components of E and H for each of the 500 x 500 rows of a cubic lattice spanning 50 wavelengths (assuming 10 cells/wavelength resolution). FD-TD time stepping would be performed via row operations mapped onto the individual CM processors. These row operations would be performed concurrently. Thus, for a fixed number of time steps, the total running time would be proportional to the time needed to perform a single row operation, which in turn would be proportional to the number of vector field components in the row, or $O(N^{1/3})$. For the 50-wavelength cubic lattice noted above, this would imply a dimensional reduction of the computational burden from $O(500^3)$ to O(500), a tremendous benefit. As a result, it is conceivable that a suitably scaled CM could model one look angle of a 50-wavelength three-dimensional scatterer in only a few seconds, achieving effective floating point rates in the order of 100 Gflops. For this reason, FD-TD algorithm development for the CM is a promising area of research.

13. CONCLUSION

Recent advances in FD-TD modeling concepts and software implementation, combined with advances in computer technology, have expanded the scope, accuracy, and speed of FD-TD modeling to the point where it may be thre preferred choice for certain types of electromagnetic wave scattering and coupling problems. This article has attempted to provide a succinct state-of-the-art review of FD-TD modeling applications. The reader is referred to the journal papers and reports listed below for details of the FD-TD algorithms and applications.

14. REFERENCES

[1] K. S. Yee, "Numerical solution of initial boundary value problems involving Maxwell's equations in isotropic media," IEEE Trans. Antennas Propagat., vol. AP-14, pp. 302-307, May 1966.

[2] A. Taflove and M. E. Brodwin, "Numerical solution of steady-state electromagnetic scattering problems using the time-dependent Maxwell's equations," IEEE Trans. Microwave Theory Tech., vol. MTT-23, pp. 623-630, Aug. 1975.

Continued on page 19

Feature Article—*Continued from page 18*

[3] G. A. Kriegsmann, "Exploiting the limiting amplitude principle to numerically solve scattering problems," Wave Motion, vol. 4, pp. 371-380, 1982.

[4] A. Taflove and M. E. Brodwin, "Computation of the electromagnetic fields and induced temperatures within a model of the microwave-irradiated human eye," IEEE Trans. Microwave Theory Tech., vol. MTT-23, pp. 888-896, Nov. 1975.

[5] A. Taflove, "Application of the finite-difference time-domain method to sinusoidal steady state electromagnetic penetration problems," IEEE Trans. Electromagn. Compat., vol. EMC-22, pp. 191-202, Aug. 1980.

[6] A. Taflove and K. R. Umashankar, "A hybrid moment method / finite-difference time-domain approach to electromagnetic coupling and aperture penetration into complex geometries," IEEE Trans. Antennas Propagat., vol. AP-30, pp. 617-627, July 1982.

[7] R. Holland, Threde: A free-field EMP coupling and scattering code," IEEE Trans. Nuclear Sci., vol. NS-24, pp. 2416-2421, Dec. 1977.

[8] K. S. Kunz and K. M. Lee, "A three-dimensional finite-difference solution of the external response of an aircraft to a complex transient EM environment: Part I- The method and its implementation," IEEE Trans. Electromagn. Compat., vol. EMC-20, pp. 328-333, May 1978.

[9] D. E. Meriwether, R. Fisher, and F. W. Smith, "On implementing a numeric Huygens' source scheme in a finite-difference program to illuminate scattering bodies," IEEE Trans. Nuclear Sci., vol. NS-27, pp. 1819-1833, Dec. 1980.

[10] G. Mur, "Absorbing boundary conditions for the finite-difference approximation of the time-domain electromagnetic field equations," IEEE Trans. Electromagn. Compat., vol. EMC-23, pp. 377-382, Nov. 1981.

[11] K. R. Umashankar and A. Taflove, "A novel method to analyze electromagnetic scattering of complex objects," IEEE Trans. Electromagn. Compat., vol. EMC-24, pp. 397-405, Nov. 1982.

[12] A. Taflove and K. R. Umashankar, "Radar cross section of general three-dimensional scatterers," IEEE Trans. Electromagn. Compat., vol. EMC-25, pp. 433-440, Nov. 1983.

[13] A. Taflove, K. R. Umashankar, and T. G. Jurgens, "Validation of FD-TD modeling of the radar cross section of three-dimensional structures spanning up to nine wavelengths," IEEE Trans. Antennas Propagat., vol. AP-33, pp. 662-666, June 1985.

[14] B. Engquist and A. Majda, "Absorbing boundary conditions for the numerical simulation of waves," Math. Comp., vol. 31, pp. 629-651, July 1977.

[15] G. A. Kriegsmann and C. Morawetz, "Solving the Helmholtz equation for exterior problems with variable index of refraction: I," SIAM J. Sci. Stat. Comput., vol. 1, pp. 371-385, Sept. 1980.

[16] A. Bayliss and E. Turkel, "Radiation boundary conditions for wave-like equations," Commun. Pure Appl. Math., vol. 33, pp. 707-725, 1980.

[17] L. N. Trefethen and L. Halpern, "Well-posedness of one-way wave equations and absorbing boundary conditions," Inst. Comput. Appl. Sci. and Eng. (ICASE), NASA Langley Res. Center, Hampton, VA, Report 85-30, June 1985.

[18] J. G. Blaschak and G. A. Kriegsmann, "A comparative study of absorbing boundary conditions," J. Comp. Physics, in press.

[19] A. Taflove and K. R. Umashankar, "The finite-difference time-domain (FD-TD) method for electromagnetic scattering and interaction problems," J. Electromagn. Waves and Appls., vol. 1, pp. 243-267, 1987.

[20] A. Taflove and K. R. Umashankar, "Analytical models for electromagnetic scattering," Final Report RADC-TR-85-87 on Air Force Contract F19628-82-C-0140, Electromagn. Sci. Division, Rome Air Development Center, Hanscom AFB, MA, May 1985.

[21] T. G. Jurgens, A. Taflove, and K. R. Umashankar, "FD-TD conformal modeling of smooth curved surfaces," Proc. 1987 URSI Radio Science Meeting, Blacksburg, VA, June 1987, p. 227.

[22] M. Fusco, "FDTD algorithm in curvilinear coordinates," submitted to IEEE Trans. Antennas Propagat.

[23] V. Shankar and W. Hall, "A time domain differential solver for electromagnetic scattering problems," Proc. 1988 URSI National Radio Science Meeting, Boulder, CO, Jan. 1988, p. 103.

[24] B. Beker, K. R. Umashankar, and A. Taflove, "Numerical analysis and validation of the combined field surface integral equations for electromagnetic scattering by arbitrary shaped two-dimensional anisotropic objects," submitted to IEEE Trans. Antennas Propagat.

[25] J. Gilbert and R. Holland, "Implementation of the thin-slot formalism in the finite-difference EMP code THREDII," IEEE Trans. Nuclear Sci., vol. NS-28, pp. 4269-4274, Dec. 1981.

[26] K. S. Yee, "A numerical method of solving Maxwell's equations with a coarse grid bordering a fine grid," SGEMP Note #9, Document D-DV-86-0008, D Division, Lawrence Livermore National Laboratory, July 1986.

[27] A. Taflove, K. R. Umashankar, B. Beker, and F. Harfoush, "Detailed FD-TD analysis of electromagnetic fields penetrating narrow slots and lapped joints in thick conducting screens," IEEE Trans. Antennas Propagat., vol. AP-36, Feb. 1988 (in press).

[28] R. Holland and L. Simpson, "Finite-difference analysis of EMP coupling to thin struts and wires," IEEE Trans. Electromagn. Compat., vol. EMC-23, pp. 88-97, May 1981.

[29] K. R. Umashankar, A. Taflove, and B. Beker, "Calculation and experimental validation of induced currents on coupled wires in an arbitrary shaped cavity," IEEE Trans. Antennas Propagat., vol. AP-35, pp. 1248-1257, Nov. 1987.

[30] D. T. Borup, D. M. Sullivan, and O. P. Gandhi, "Comparison of the FFT conjugate gradient method and the finite-difference time-domain method for the 2-D absorption problem," IEEE Trans. Microwave Theory Tech., vol. MTT-35, pp. 383-395, April 1987.

[31] D. M. Sullivan, D. T. Borup, and O. P. Gandhi, "Use of the finite-difference time-domain method in calculating EM absorption in human tissues," IEEE Trans. Biomed. Engrg., vol. BME-34, pp. 148-157, Feb. 1987.

[32] D. M. Sullivan, O. P. Gandhi, and A. Taflove, "Use of the finite-difference time-domain method in calculating EM absorption in man models," IEEE Trans. Biomed. Engrg., vol. BME-35, 1988 (in press).

Continued on page 20

Feature Article—*Continued from page 19*

[33] C.-Q. Wang and O. P. Gandhi, "Numerical simulation of annular phased arrays for anatomically-based models using the FDTD method," submitted to IEEE Trans. Microwave Theory Tech.

[34] X. Zhang, J. Fang, K. K. Mei, and Y. Liu, "Calculations of the dispersive characteristics of microstrips by the time-domain finite difference method," IEEE Trans. Microwave Theory Tech., vol. 36, pp. 263-267, Feb. 1988.

[35] D. H. Choi and W. J. R. Hoefer, "The finite-difference time-domain method and its application to eigenvalue problems," IEEE Trans. Microwave Theory Tech., vol. MTT-34, pp. 1464-1470, Dec. 1986.

[36] W. K. Gwarek, "Analysis of arbitrarily-shaped two-dimensional microwave circuits by the finite-difference time-domain method," IEEE Trans. Microwave Theory Tech., vol. 36, 1988 (in press).

[37] F. Harfoush, A. Taflove, and G. A. Kriegsmann, "A numerical technique for analyzing electromagnetic wave scattering from moving surfaces in one and two dimensions," submitted to IEEE Trans. Antennas Propagat.

[38] D. De Zutter, "Reflections from linearly vibrating objects: plane mirror at oblique incidence," IEEE Trans. Antennas Propagat., vol. AP-30, pp. 898-903, Sept. 1982.

[39] K. R. Umashankar, S. K. Chaudhuri, and A. Taflove, "Finite-difference time-domain formulation of an inverse scattering scheme for remote sensing of inhomogeneous lossy layered media," submitted to IEEE Trans. Antennas Propagat.

[40] M. A. Strickel, A. Taflove, and K. R. Umashankar, "Accurate reconstruction of two-dimensional conducting and homogeneous dielectric target shapes from a single-point TM scattered field pulse response," submitted to IEEE Trans. Antennas Propagat.

[41] M. A. Strickel and A. Taflove, "Reconstruction of one- and two-dimensional inhomogeneous dielectric targets using the FD-TD / feedback method," in preparation.

[42] C. L. Bennett and G. F. Ross, "Time-domain electromagnetics and its applications," Proc. IEEE, vol. 66, pp. 299-318, March 1978.

Editor's Comments—*Continued from page 4*

managed, it has no reserve capacity. If even one of a rather large number of employees is ill or quits, the result is a disproportionately large effect. The contingency plans either don't work or don't exist. One of the more frustrating experiences occurred with the February issue. Because of the January URSI meeting, everyone worked very hard to get the material off to New York by the usual deadline. It "sat", with nothing being done, for at least a week and one-half after it arrived. This issue will serve as something of a test. If New York can be responsive, great. If not, we may have to examine other alternatives for getting the *Newsletter* out on time. I'll be making a full report at the June AdCom meeting. "Stay tuned", and I welcome any suggestions or comments.

On a much brighter note, your *Newsletter* has turned 30! Actually, the February issue was issue 1 of the thirtieth volume, but I understand that publication was not begun at the start of a year. I have had the feeling that something should appear in these pages to celebrate since I started thinking about the significance of this, last Fall, but I can't come up with a good idea (any suggestions?). Perhaps that is as it should be. We'll simply keep doing the best job we can, and be pleased with the growth and vitality of our society. Please note that I never use the so-called "editorial we". The "we" refers to the Associate Editors, officers, authors, and other members and supporters of AP-S -- and our readers -- who put a great deal of time and effort into this *Newsletter*. Thank you very much, one and all. I hope to see as many of you as possible at Syracuse in June. Best wishes until then.

Ross

Feature Articles Solicited

Ercument Arvas
Dept. of Electrical and Computer Engineering
Syracuse University
Syracuse, NY 13244-1240
(315) 423-2655

Richard Compton
Dept. of Electrical Engineering
Phillips Hall
Cornell University
Ithaca, NY 14853
(607) 255-9231

The AP-S *Newsletter* continues to actively solicit feature articles which describe engineering activities taking place in industry, government, and universities. Emphasis is placed on providing the reader with a general understanding of either a particular technical area, or of the technical problems being addressed by various engineering organizations as well as their capabilities to cope with these problems. If you are interested in submitting an article, please contact either Ercument Arvas or Richard Compton to discuss the appropriateness of the topic.